Metallization of silicon in a shock wave: the metallization threshold and ultrahigh defect densities

2004 J. Phys.: Condens. Matter 16 8139

(http://iopscience.iop.org/0953-8984/16/46/003)

INSTITUTE OF PHYSICS PUBLISHING JOURNAL OF PHYSICS: CONDENSED MATTER

J. Phys.: Condens. Matter **16** (2004) 8139–8153 PII: S0953-8984(04)82517-7

Metallization of silicon in a shock wave: the metallization threshold and ultrahigh defect densities

S D Gilev[1] **and A M Trubachev**[2]

Lavrentyev Institute of Hydrodynamics, Lavrentyev prospekt 15, Novosibirsk 630090, Russia

E-mail: gilev@hydro.nsc.ru

Received 18 June 2004
Published 5 November 2004
Online at stacks.iop.org/JPhysCM/16/8139
doi:10.1088/0953-8984/16/46/003

Abstract

Time-resolved electrical conductivity measurements on monocrystalline doped silicon are performed under shock compression up to 23 GPa followed by release. With increasing normal stress, the electrical conductivity of silicon increases monotonically by five orders of magnitude and reaches that of 'poor' metals. The stress dependence of the conductivity comprises two parts: a steep rise and a 'plateau'. The 'plateau' conductivity corresponds to the metallic state of silicon; it does not depend on the compression regime or the doping type or amount of impurity. The onset of the metallic phase corresponds to a shock stress of about 10 GPa; most of the specimen is metallic at 12 GPa. The state of shock-compressed silicon proves to be extremely defective. The defect concentration in shocked silicon exceeds the equilibrium concentration by five orders of magnitude and exceeds the defect concentration in classic metals by an order of magnitude. This indicates distinctive features of brittle solid deformation. Experimentally, the metallic phase proves to be metastable. Releasing stress causes a temporary delay of the reverse transition.

List of symbols

P_x	Stress
σ	The electrical conductivity
τ	The characteristic time of current relaxation
$L_s L_x$	The shunt inductance and specimen inductance, respectively
$R_s R_x$	The shunt resistance and specimen resistance, respectively
V	Voltages through the electrodes
V_0	Initial voltages through the electrodes

[1] Author to whom any correspondence should be addressed.
[2] Present address: Yugorsk Physico-Mathematical School, ulitsa Mira 151, Hanty-Mansiysk 628011, Russia.

h_s	Thickness of the shunt
h	The thickness of the specimen
k	The compression factor of the specimen
ρ_c	The constantan resistivity
t_h	The hydrodynamic relaxation time
x_0	The total thickness of the shunt–specimen system
D	The shock velocity
U	The mass velocity
t_e	The electromagnetic relaxation time
μ_0	The magnetic permeability of vacuum
t	The time
a, b	Coefficients in the linear dependence of the shock velocity on the mass velocity
ρ_0	The initial specific resistance of the specimen
P_x^1	The stress of the first shock wave in silicon (estimated by the impedance matching method)
V_T	The specific volume corresponding to the onset of the phase transformation
V_0	The initial specific volume
ρ_{shock}, ρ_{static}	Resistivities at shock and static compression
$\Delta\rho_T$	The difference due to the temperature effect
$\Delta\rho_{def}$	The difference due to the generation of shock defects
T	The temperature
T_0	The initial temperature
γ_0	The Grüneisen factor under standard conditions
γ	The Grüneisen factor
θ	The Debye temperature
α	The thermal resistance factor
n_v	The vacancy concentration
ρ_v	The metal resistivity caused by a defect concentration of 1%
ε	The deformation
n_v^e	The equilibrium concentration of crystal defects
E	The energy of the defect
k	The Boltzmann factor

1. Introduction

The metallization phenomenon is defined as an inherent action of high pressure on condensed matter. The metallic state is versatile at sufficiently large compression of semiconductors and dielectrics. At present the metallization is of great importance in studying planet magnetism. Silicon is a classic object of research in high pressure physics. Interest in the study is due to the global abundance of the element in the Earth's crust and its great importance in electronics. Diffraction measurements under static compression [1–11] have provided the most detailed description of the physical behaviour of silicon. At present, the sequence of phase transitions under hydrostatic compression appears to comprise the following phases: cubic diamond Si I (stable from ambient pressure to 13 GPa), metallic β-tin Si II (11–14 GPa) [1, 3, 5, 6, 8, 10], orthorhombic Si (13–16 GPa) [10], simple hexagonal Si V (15–

35 GPa) [4–6, 10], orthorhombic Si VI (35 GPa) [4, 9, 11], hexagonal close packed Si VII (40 GPa) [4, 6], face centred cubic Si X (78 GPa) [8]. Following release, body centred cubic Si III [2] and two tetragonal phases, Si VIII, Si IX [7], are found. There are regions of coexistence of different phases; therefore the transition pressures are defined somewhat indefinitely [3–5]. Theoretical research predicts quite well the transition parameters in equilibrium [12]. The metallic transition from the diamond phase to the β-tin one has also been studied by spectroscopic [13, 14] and electric [15, 16] techniques. Electrical measurements by Bundy and Kasper [16] have shown that the electrical conductivity of silicon increases monotonically with pressure P and attains the conductivity of metals such as Ni, Zn, Mo at $P \approx 15$ GPa (on Drickamer's reference point scale [17]). Resistance measurements have shown that silicon becomes a superconductor at high pressure [18].

Shock wave investigations of silicon [19–25] have been less comprehensive and not necessarily mutually correlated. Pavlovskii [19] found a three-wave structure caused by the Hugoniot elastic limit (HEL), the phase transition and the driving stress. The normal stress of the phase transition to metal was derived as 11.2 GPa for a shock wave propagating in the (111) crystal direction. Gust and Royce [20] performed a thorough study of shock profiles for (100), (111), (110) directions. Phase transitions were found at stresses of about 10 and 13–14 GPa (the (100) direction had the maximum HEL and the lower transition could not be resolved). Coleburn *et al* [21] studied polarization, electrical resistance and shock profiles. From the resistance decrease it was concluded that the metallic state occurred at stresses exceeding the HEL (5.5 GPa). On further increasing the shock stress, the resistance rose considerably. At the same time the transition stress derived from the wave profile was found as 13 GPa. Resistance measurements taken by Rosenberg [22] under elastic compression were in agreement with predictions of the energy band theory. A metallic transition was observed in the neighbourhood of the HEL (5.6 GPa). German and Poduretc [23] conducted x-ray analysis of specimens recovering from shock and found the initial diamond phase only. The Hugoniot of monocrystalline silicon was found by Goto *et al* [24]. The HEL stresses were found to be 8.4 GPa for the (100) direction and 5.6 GPa for (110), (111) directions. The phase transition stress was determined as $P_x = 13.4 \pm 0.2$ GPa independently of the crystallographic direction. A comparison of the data with the hydrodynamic model showed that above the HEL silicon lost its shear strength and transformed to the isotropic state. Zaporozhetc [25] measured the reflectivity of silicon and estimated the stress for the metallic transition as 15 GPa. After release, the specimen continued to reflect light, which indicates conservation of the metallic state.

At present there is a vast discrepancy between experimental data on static and shock compression. On the one hand, under static compression the metallic transition is reliably registered by various methods at pressures of 11–12 GPa [3, 5, 6, 10, 11, 13–16]. On the other hand, in dynamic conditions the transition stress lies in the range from 5.5 GPa [21, 22] to 15 GPa [25]. Such a discrepancy cannot be explained by experimental errors; it indicates methodology problems in the dynamic measurements. At present there are no direct measurements of the electrical conductivity which might let one uniquely determine the onset of the metallic transition of silicon in a shock wave.

The objective of this paper is to study experimentally the transformation of monocrystalline silicon into the metallic state under shock compression. We are interested in the metallization threshold and the nature and parameters of the metallic state. It is important to understand the distinctive features of the dynamical metallization as compared to the static case.

In addition to the fundamental aspects, interest in shock metallization is stimulated by a number of applications. At present shock-induced conductivity is used for generating and governing electromagnetic energy flows in high power systems: generators of electromagnetic

energy density [26–28], current switches [29, 30], generation of radiation pulses [31]. This paper advances previous investigations in the field [32, 33] and covers recent results.

2. Experimental procedure

2.1. A scheme for measuring the electrical conductivity in the dielectric–metal transition

The problems in measuring the electrical conductivity in the dielectric–metal transition in a shock wave were already known of in the early 1960s. The electrical contact technique is the one in most widespread use for this purpose [34–37]. The measuring circuit comprises a shunt and a specimen connected in parallel to one another. Electric current is produced by an external source and remains constant for the measuring time. Initially, the current flows through the shunt. As a shock wave arrives, the specimen is switched to the shunt; the current redistributes between the shunt and the specimen. The characteristic time of the current relaxation in the circuit is $\tau = (L_s + L_x)/(R_s + R_x)$, where L_s and L_x are the shunt inductance and specimen inductance, respectively, and R_s and R_x are their resistances. The time τ determines the temporal resolution of the electric circuit. To gain good accuracy in the measurement it is essential to use a shunt resistance which is near the specimen one, i.e. $R_s \approx R_x$. If the specimen conductivity is high, so will the relaxation time τ be. For a metallic specimen, the time τ exceeds the lifetime of the shock stress ($\sim$1 μs). To investigate metallization one has to decrease the inductance of the shunt–specimen circuit. In the early studies [34–37] the shunt was placed outside the shock zone and the measurement loop was rather large. The relaxation time in the circuit was considerably reduced by Nabatov *et al* [38, 39] by locating the shunt close to the specimen, inside the shock zone. The highest conductivity was $\approx 2 \times 10^3\ \Omega^{-1}\ \mathrm{cm}^{-1}$ [38, 39] and corresponded to the temporal resolution $\sim$0.5 μs. Close conductivity was registered in accurate experiments by Nellis *et al* [40] on fluid hydrogen. Nellis *et al* [40] stated that the temporal resolution was determined by the magnetic field diffusion in the compressed specimen. Actually the electrical transients in the shunt–specimen circuit take more time and limit the resolution. The experimental record of the voltage [40, figure 3] can be described by an electrical engineering model with the characteristic time $\tau \approx 50$ ns. The temporal resolution of the measurements is highly dependent on the conductivity; it falls off at larger conductivity. The conductivity of classic metals is two orders of magnitude larger than that registered in [38–40]. In this case, using the known schemes [38–40] leads to a catastrophic decrease of the temporal resolution, which turns out to not be suitable for the shock wave method. To solve this problem one has to substantially reduce the inductance of the shunt–specimen circuit.

The necessary improvement of the measuring scheme can be attained by bringing the shunt and the specimen extremely close [32]: the shunt (constantan foil, 100–200 μm thick, 10 mm wide) is superimposed on the specimen and contacts with it over the entire surface (figure 1(a)). Electrodes (made of copper or constantan wires pressed to about 15 μm thick) are spot-welded onto the foil. The electrode base is usually 6 mm. The electrodes and the foil are placed in the same plane; they are connected in a measuring cable outside the shock zone. The electrical circuit is shown in figure 1(b). A power supply charges a capacitor C prior to the experiment. A thyristor switches on and current starts to flow through an inductance L and the measuring cell (the shunt resistor R_s in parallel with the specimen resistor R_x). The current is registered by an inductive-type gauge. At the moment of current maximum (the current rise time is about 70 μs) a shock wave enters the cell. The electrical current in the circuit (up to 700 A) is practically constant during the measuring stage.

The distinctive features of the cell are the following: (1) the inductance of the shunt–specimen circuit and the relaxation time τ are minimal; (2) the current flows into the specimen

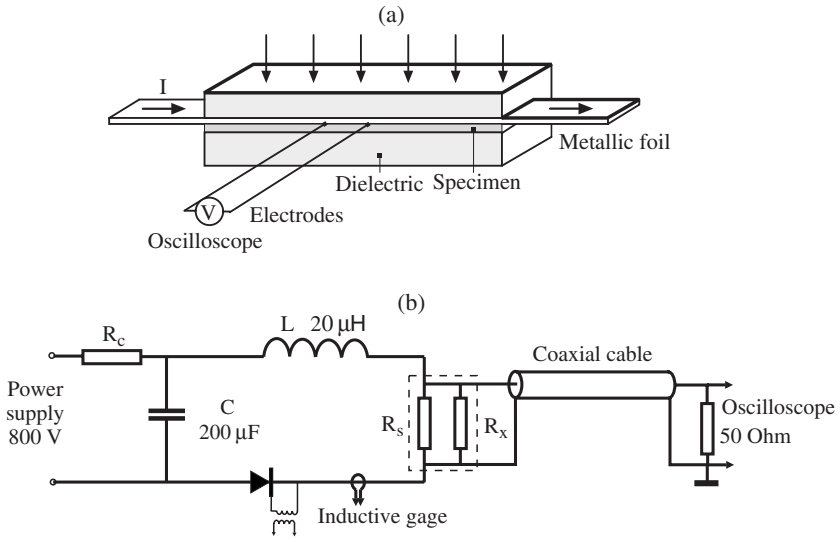

Figure 1. A schematic diagram of the experiments measuring the electrical conductivity in the dielectric–metal transition in a shock wave: the measuring cell (a) and the complete electrical circuit (b). The cell (a) corresponds to a part of the circuit (b) marked by the dashed line. A plane shock wave propagates over the cell from the top down. The voltage from the shunt–specimen interface is recorded by an oscilloscope.

at its edges and therefore current lines are well defined by the centre of a long specimen; (3) the shunt contacts with the specimen over the interface and hence the effect of the contact resistance is low; (4) the direction of wave propagation is perpendicular to the current flow and therefore there is no polarization.

To obtain the conductivity, two states of the specimen are used: the initial state (just prior to shock compression) and the final one (on completing the transients). Let these states correspond to voltages through the electrodes of V_0 and V. Considering a circuit of two resistances in parallel (a shunt and a specimen) one can obtain the electrical conductivity of the shock-compressed specimen:

$$\sigma = \frac{h_s k}{h}\frac{1}{\rho_c}\left(\frac{V_0}{V} - 1\right). \tag{1}$$

Here h_s is the thickness of the shunt, h is the thickness of the specimen, k is the compression factor of the specimen, ρ_c is the constantan resistivity. In formula (1) it is assumed that the current flow is one-dimensional and that the total current and the shunt resistance are constant during the measurements.

The temporal resolution of the cell is determined by the hydrodynamic and electromagnetic transients. The hydrodynamic relaxation is caused by reverberation of the stress in the shunt–specimen system surrounded by a thick dielectric. It takes a characteristic time of $t_h \approx 2x_0/D$ (x_0 is the total thickness of the system, D is the shock velocity). The electromagnetic relaxation time is $t_e \approx \mu_0 \sigma x_0^2$. To perform accurate measurements, the relaxation times have to be much less than the observation time t_h, $t_e \ll t$. Considering as typical values $t \approx 1\ \mu$s, $D \approx 5$ km s^{-1}, $\sigma \approx 5.9 \times 10^5\ \Omega^{-1}$ cm^{-1} (the copper conductivity), one can deduce that the layer thickness has to be much less than 100 μm. Thus unlike the known schemes, the present scheme allows one to measure the electrical conductivity up to the copper one.

2.2. Details of the experiment

Constantan foil was used as a shunt. This choice was guided by the slight change of the electrical resistance of constantan under shock compression [41]. Tests showed that shock compression caused electromagnetic transients in metal [42]. On their completion, the constantan resistance increased slightly (2–3% at the stress $P_x \approx 20$ GPa). Therefore this effect was thereafter neglected.

The specimens of silicon were plates 0.23–0.41 mm thick, 10 mm wide and about 30 mm long. The specimen surfaces, of mirror quality, were parallel to the crystallographic plane (100). The specimens had resistivity 0.1–50 Ω cm at room temperature and different types of impurity conductance (n-type doped with phosphorus and p-type doped with boron). The specimen conductivity was extrinsic up to 450 K at ambient pressure.

Loading of the cell was realized in two ways: a plane wave generator contacted the cell or high explosive accelerated a metallic plate which struck the cell. To vary the stress, the attenuation systems including layers of widely different shock impedances were used. The shunt and specimen thicknesses were much less than the thickness of the holding dielectric (generally Micarta). Therefore the stress P_x in the specimen was identified with the appropriate stress in the dielectric (on completing the wave reverberation). The specimen state was derived by the impedance matching method. Hugoniots of materials were given as linear dependences of the shock velocity D on the mass velocity U: $D = a+bU$. The following material constants were used: copper—$a = 3.915$ km s^{-1}, $b = 1.495$ [43]; constantan—$a = 4.24$ km s^{-1}, $b = 1.55$ [44]; aluminium alloy D16T—$a = 5.041$ km s^{-1}, $b = 1.42$; stainless steel—$a = 4.57$ km s^{-1}, $b = 1.49$; Micarta—$a = 3.048$ km s^{-1}, $b = 1.422$ [45]; glass Textolite—$a = 2.5$ km s^{-1}, $b = 1.89$ [46]. To find the compression factor of silicon, the experimental data from [24] were used. Loading parameters were monitored in a number of experiments by measuring the shock stress P_x by the manganin gauge technique. The maximum stress in the experiments performed for sufficiently small total thickness of the layers was quite appropriate for the impedance matching method.

A test of the measurement scheme was made in special experiments wherein a reference conductor was placed into the cell instead of silicon. The reference was initially separated from the shunt by a small air gap. A shock wave provided electrical switching of the reference to the shunt. The experiments were performed with references of different thickness. For a thin reference (constantan or copper foil, 50–200 μm thick) the experimental voltage was compared with the electrical engineering model. For a thick reference (copper plate, 3 mm thick) the time dependence of the voltage was compared with results of 1D modelling of the magnetic field diffusion in the cell. The experiments of the two types gave the expected results, which has given confidence in the correctness of the measuring technique.

3. Experimental results

3.1. Metallization in a shock wave

A number of typical oscillograms taken in the experiments are shown in figure 2. Included here are three voltage records from the conductivity cell and corresponding stress records. The stress records were obtained using a manganin gauge as usual in separate experiments. In such experiments, the manganin gauge was placed in the cell in place of the shunt–specimen system. The stress error is estimated to be of 5%. The record set fits increasing shock stress.

Figure 2(a) gives the records of an experiment corresponding to the lowest shock stress (3 GPa). At shock stress below 10 GPa the conductance of silicon proved to be quite small.

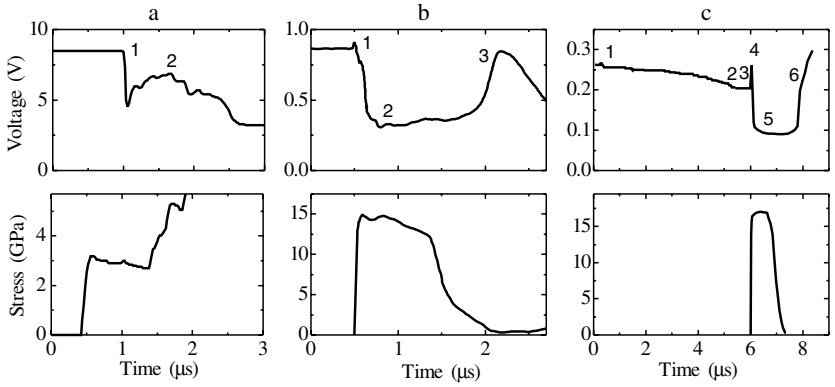

Figure 2. The experimental records: the voltage from the conductivity cell (top); the stress registered by a manganin gauge (bottom). (a) A layer attenuation system (experiment No 596). The stress of the first shock wave in a dielectric is $P_x \approx 3$ GPa. The following labels mark the arrival of shock waves at the specimen: 1—the first wave; 2—the second one. The silicon conductivity up to moment 2 is found as $\sigma \approx 0.5\ \Omega^{-1}\ \mathrm{cm}^{-1}$. (b) A charge of high explosive in contact with the cell (experiment No 398). The shock stress is $P_x \approx 14.8$ GPa; the conductivity of the shocked silicon is $\sigma = (3.0 \pm 0.3) \times 10^4\ \Omega^{-1}\ \mathrm{cm}^{-1}$. The following moments are marked: arrival of a shock wave at the specimen, 1; the metallic state of silicon, 2; arrival of the non-axial release wave, 3. (c) Loading with a metal impacter (experiment No 552), $P_x \approx 17$ GPa, $\sigma \approx (3.5 \pm 0.2) \times 10^4\ \Omega^{-1}\ \mathrm{cm}^{-1}$. The following times are marked: the impacter begins to move, 1; the impacter strikes a dielectric, 2; a shock wave arrives at a shunt, 3; the occurrence of silicon conductance, 4; the metallic state of silicon, 5; arrival of a non-axial release wave, 6.

For this stress range the measurements were performed with a shunt separated from a specimen like in known schemes [34, 38–40]. In the measurement a load system produces a sequence of compression waves of increasing amplitude. The manganin gauge is placed in the path of propagation of a shock wave at 1.5 mm from a specimen. The silicon specimen attains its equilibrium state during the shock reverberation. The shock impedance of silicon is larger than that of the surrounding dielectric; therefore the initial stress in silicon exceeds the incident wave stress. Under shock reverberation the stress in silicon is taken as equal to the stress in the dielectric. The voltage record displays the compression history of the specimen: the conductivity occurs at the first compression (the moment labelled as 1); on relaxing the stress, the voltage increases and the specimen conductivity decreases. This indicates the reversibility of the silicon behaviour under compression and release in the elastic stress range. The electrical conductivity may be estimated at the moment just before arrival of the second shock wave at the specimen (label 2). The second shock wave has higher stress and produces higher conductivity.

Figure 2(b) represents an experiment performed at larger stress ($P_x \approx 14.8$ GPa) when the measuring cell (figure 1(a)) was used. As is seen from the record, the arrival of a shock wave at the silicon (label 1) causes the occurrence of high conductance. An abrupt voltage drop is mostly preceded by a small peak caused by the electromagnetic transients in the shocked constantan foil [42]. Upon completing the transients, the voltage is characteristic of the metallic state of silicon (label 2). Later, the voltage changes slightly and is consistent with the stress decrease. A subsequent drastic rise of the voltage takes place in a rarefaction wave. On unloading, the signal often becomes unpredictable, which may be due to the effect of non-axial tensile waves.

Figure 2(c) shows oscillograms taken in an experiment that involved loading the cell using a metallic impacter. In that case the signal is more complex. The electrical current

flowing in a shunt generates a magnetic field; therefore the motion of the metallic conductor produces changes in the magnetic flux through the measuring circuit. As a result, a spurious voltage is recorded by an oscilloscope. The stray magnitude depends on the velocity of the metallic plate relative to the shunt, the shunt conductance and the system geometry. The stray voltage is negative when bringing the plate and the shunt close to one another; the voltage changes sign on separating the elements from each other. The additional voltage complicates the measurements. Moreover, this signal is a useful time marker. The impacter starts to move at the moment designated 1. The impacter acceleration and its convergence with a shunt tend to decrease the voltage. At the moment 2, the impacter strikes the dielectric. A shock wave propagates through the dielectric; at the moment 3, the shock wave reaches the shunt. The shunt attains the velocity of the dielectric. The relative velocity of the impacter and the shunt is reduced to zero; the voltage increases up to the initial value at 4. Then the silicon conductivity arises and the voltage decreases sharply. By the moment 5 the cell transients are completed; a steady voltage characterizes the conductive state of silicon.

Distinctive features of the records permit one to relate instants of shock arrival and conductance rise. The appearance of the conductance corresponds well to the entry of the shock wave into the specimen. The temporal resolution of the conductivity measurements is about 200 ns at the highest conductivity. At such times a steady voltage is established. Notice that a sharp drop of the voltage indicates conclusively that appreciable conductivity occurs for less time.

The results of the experiments measuring the conductivity of monocrystalline silicon are summarized in table 1. Presented here is information on the type of loading, layer materials, the conductivity cell, the shunt resistance R_s (for low stress experiments where the shunt was spatially separated from the specimen), the initial specific resistance of the specimen ρ_0, the normal stress P_x in a dielectric, the stress of the first shock wave in silicon P_x^1 (estimated by the impedance matching method), the electric conductivity of the compressed silicon σ.

Four experiments at the shock stress of 20.2 GPa give conductivities of $(4.4 \pm 0.3) \times 10^4\ \Omega^{-1}\ \mathrm{cm}^{-1}$. The relatively small standard error manifests the good reliability of the measuring scheme. The conductivity exceeds the maximum one measured in the dielectric–metal transition [38–40] by more than one order of magnitude. The temporal resolution of the measurements is better than [38, 39] but it is nominally worse than in the accurate measurements of Nellis *et al* [40]. As pointed out in section 2.1, the temporal resolution is highly dependent on the conductivity. The accuracy and temporal resolution decrease drastically when measuring the metallic conductivity. Therefore we can state that the present data have sufficiently good accuracy as well as the temporal resolution.

In the experiments the specimen thickness varies about 1.8-fold and the conductivity proves to be thickness independent. This demonstrates the negligible effect of an oxide layer at the silicon surface. This is also confirmed by experiment No 436 conducted with a two-layer specimen. The additional interface does not affect the conductivity, which is within the scatter range of experiments Nos 375, 397, 398.

Unlike experiments corresponding to the stresses 14.8 and 20.2 GPa, four tests at $P_x \approx 10$–10.5 GPa show a wide scatter of results. This may be explained by the very sharp character of the conductivity dependence on the shock stress. In such cases stochastic variation in loading conditions can produce large differences in the physical state of the specimen.

A number of experiments were performed using the more rigid dielectric (glass Textolite). The results of these experiments agree well with the main experiment series. So, the effect of the loading history on the specimen conductivity is not marked.

To determine the nature of the conductivity, the effect of impurity on the electrical conductivity was considered. Impurities fully defined the electrical properties of the specimens under ambient pressure. Experiments Nos 551, 553, 554 were conducted with specimens

Table 1. The experimental results from measuring the electrical conductivity of monocrystalline silicon under shock loading. (The following notation is used: ρ_0—the initial resistivity; P_x—the normal stress in a dielectric; P_x^1—the stress estimated for the first shock wave in silicon; σ—the conductivity of the compressed silicon; R_s—the resistance of a shunt separated from a specimen.)

Exp. Nos	Loading[a]	Configuration of the layer system: material[b] (thickness (mm))	Cell[c] (R_s Ω)	ρ_0 (Ω cm)	P_x (GPa)	P_x^1 (GPa)	σ (Ω^{-1} cm^{-1})
546	C	Cu(5.1)–M(4.8)–Cu(5)–M(1.5)–Si(0.29)–M(7.5)	1 (10.4)	7.4	3	5.3	0.5 ± 0.2
596	C	Cu(5.1)–M(4.8)–Cu(5)–M(3)–Si(0.28)–M(9.5)	1 (30.8)	6.7	3	5.3	0.37 ± 0.03
545	C	Cu(5.1)–M(4.8)–Cu(5.1)–M(3.1)–Si(0.28)–M(10.2)	2 (3.03)	6.0	3.9	6.9	5.1 ± 0.9
420	C	Cu(5.9)–M(6.1)–Al(5.9)–M(3.4)–Si(0.36)–M(7)	2[d]	∼5	6.2	10.1	$(4.4 \pm 1.5) \times 10^1$
544	C	Cu(5.1)–M(3.1)–Si(0.29)–M(9)	2 (3.0)	4.8	7.5	12.0	$(1.7 \pm 0.2) \times 10^2$
620	C	Cu(5.0)–M(3.2)–Si(0.27)–M(10.7)	2 (1.42)	4.5	7.5	12.0	$(1.3 \pm 0.2) \times 10^2$
399	C	Cu(6)–M(3.5)–Con(0.1)–Si(0.28)–M(3.5)	3	∼5	10	12	$(1.6 \pm 0.5) \times 10^3$
549	C	Cu(9.2)–M(3.1)–Con(0.105)–Si(0.41)–M(5.5)	3	6.7	10	12	$(7.2 \pm {}^{2}_{1.6}) \times 10^3$
374	C	Cu(3.0)–M(3.5)–Con(0.2)–Si(0.28)–M(5.5)	3	∼5	10.5	12.5	$(4.1 \pm 1.5) \times 10^3$
590	C	Cu(5.1)–M(1.5)–Con(0.1)–Si(0.395)–M(5.5)	3	46	10.5	12.5	$(1.3 \pm 0.2) \times 10^4$
428	C	St(6.2)–M(6.2)–Con(0.1)–Si(0.23)–M(10)	3	∼5	10.9	13	$(9.9 \pm 1) \times 10^3$
547	C	St(6.2)–M(3.2)–Con(0.105)–Si(0.28)–M(5.6)	3	6.5	11.4	13.2	$(1.0 \pm 0.1) \times 10^4$
401	C	Al(2.9)–M(3.5)–Con(0.1)–Si(0.28)–M(7.9)	3	∼5	12.3	14.1	$(2.5 \pm 0.15) \times 10^4$
375	C	M(3.5)–Con(0.2)–Si(0.27)–M(3.5)	3	∼5	14.8	15.8	$(3.2 \pm 0.2) \times 10^4$
397	C	M(3.5)–Con(0.2)–Si(0.27)–M(3.5)	3	∼5	14.8	15.8	$(3.6 \pm 0.5) \times 10^4$
398	C	M(5.1)–Con(0.2)–Si(0.28)–M(3.5)	3	∼5	14.8	15.8	$(3.0 \pm 0.3) \times 10^4$
436[e]	C	M(6.3)–Con(0.1)–Si(0.27 + 0.27)–M(3.9)	3	∼5	14.8	15.8	$(3.1 \pm 1) \times 10^4$
405	C	Al(5.8)–M(8.0)–Con(0.2)–Si(0.27)–M(7.0)	3	∼5	15.3	15.7	$(3.1 \pm 0.3) \times 10^4$
583	F	M(3.1)–Con(0.19)–Si(0.3)–M(12.5)	3	4.3	15.5	15.9	$(3.7 \pm {}^{0.8}_{0.6}) \times 10^4$
552	F	M(3.2)–Con(0.2)–Si(0.29)–M(3.5)	3	4.15	17.0	17.3	$(3.5 \pm 0.2) \times 10^4$
581	F	M(4.8)–Con(0.2)–Si(0.36)–M(12.2)	3	5.0	17.0	17.3	$(3.7 \pm 0.5) \times 10^4$
586	F	M(4.7)–Con(0.2)–Si(0.29)–M(12.3)	3	5.7	17.0	17.3	$(3.7 \pm {}^{1.0}_{0.7}) \times 10^4$
611	C	GT(5.8)–Con(0.19)–Si(0.31)–GT(8.8)	3	∼5	17.2	17.5	$(3.4 \pm {}^{0.4}_{0.3}) \times 10^4$
368[f]	C	M(3.5)–Con(0.2)–Si(0.265)–M(3.5)	3	∼5	20.2	19.7	$(4.4 \pm 0.8) \times 10^4$
551	C	M(3.1)–Con(0.18)–Si(0.38)–M(5.5)	3	4.1	20.2	19.7	$(4.7 \pm 0.6) \times 10^4$
553	C	M(3.1)–Con(0.18)–Si(0.26)–M(5.5)	3	1.3	20.2	19.7	$(4.2 \pm 0.3) \times 10^4$
554	C	M(3.1)–Con(0.18)–Si(0.30)–M(5.5)	3	12.2	20.2	19.7	$(4.3 \pm 0.4) \times 10^4$
597	C	GT(8.7)–Con(0.19)–Si(0.26)–GT(7.9)	3	0.11	23.2	21.2	$(4 \pm {}^{0.8}_{0.6}) \times 10^4$
601	C	GT(4.4)–Con(0.19)–Si(0.30)–GT(3.8)	3	8.1	23.2	21.2	$(4.5 \pm {}^{0.6}_{0.5}) \times 10^4$

[a] Two types of loading are used: C—high explosive is in contact with the conductivity cell; F—a steel flyer accelerated by high explosive detonation products strikes the cell.

[b] The notation for the materials used: Cu—copper; Al—aluminium alloy D16T; Si—silicon; M—Micarta; GT—glass Textolite; Con—constantan; St—steel. The layer thickness is shown in parentheses.

[c] The notation for the conductivity cell used: 1—the shunt is remote from the shock wave zone; 2—the shunt is a constantan wire placed inside the shock zone (the shunt resistance is shown in parentheses); 3—the conductivity cell shown in figure 1(a).

[d] The shunt is a constantan foil, 1.35 mm wide, 0.1 mm thick, placed on the specimen.

[e] The silicon specimen consists of two layers.

[f] Electrodes are connected to the shunt at a surface which is opposite to the surface where the specimen is attached.

whose initial resistivities vary over one order of magnitude. As can be seen from table 1, the conductivities of shocked specimens prove to be practically the same. Also, we did not note any effect of the initial conductance type on the electrical conductivity of the compressed silicon. Thus, the high conductivity of silicon is of intrinsic nature.

The stress dependence of the electrical conductivity is represented on two scales: logarithmic (figure 3) and linear (figure 4) ones. For improved presentation, most of the data at the same compression are averaged and shown in figure 3 as one point. As can be seen

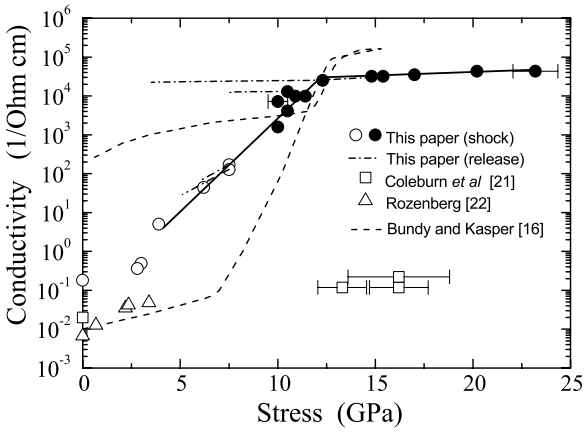

Figure 3. The dependence of the logarithm of the conductivity lg σ on the shock stress P_x for silicon. The circles and the chain curves mark results from this study. The closed circles correspond to the scheme of figure 1(a). The open circles denote data corresponding to a scheme which is analogous to that of [38–40] (the shunt and the specimen are separated spatially). The solid curve is a guide for the eye only. The chain curves correspond to the release experiments. The squares mark data evaluated by Coleburn *et al* [21]; the triangles represent the data from Rosenberg [22] reassessed to give the conductivity (in both cases, for shock compression). The broken curve denotes static compression measurements by Bundy and Kasper [16] (loading and release) corrected according to the Drickamer pressure scale [17].

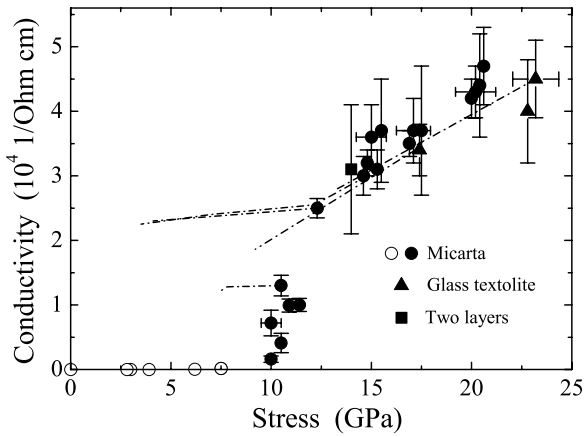

Figure 4. The dependence of the conductivity σ on the shock stress P_x. The experiments used Micarta (circles) or glass Textolite (triangles) as the dielectric and for the specimen holder. The square marks an experimental result obtained using a two-layer specimen. The chain curves correspond to release.

from the figure, on varying the stress P_x, the silicon conductivity σ increases monotonically by more than five orders of magnitude. One can discern two principal parts in the dependence $\lg\sigma(P_x)$: a steep rise and a very slow one. In the first part the logarithm of the conductivity depends almost linearly on the stress. By convention, the second part may be characterized as a 'plateau'. The maximum conductivity of silicon matches that of a 'poor' metal such as lead. The change of slope of the $\lg\sigma(P_x)$ dependence is fixed at $P_x \approx 12$ GPa.

In figure 3 also given are data obtained elsewhere: the $\sigma(P)$ dependence obtained by Bundy and Kasper [16] under static compression and the evaluations from the shock

experiments of Coleburn *et al* [21] and Rosenberg [22]. The static data [16] are presented taking account of a recalibration of the pressure scale made in 1970 [17]. The shock data [21, 22] were reprocessed to find the conductivity on the basis of the specimen dimensions and the resistance change published in the original papers.

On the basis of the experimental data, a number of conclusions can be drawn.

(1) The conductivity calculated from the data of Coleburn *et al* [21] differs from our data and the static compression data [16] by more than five orders of magnitude. It follows that the scattered signal [21] at $P_x > 10$ GPa is unrelated to the shock-induced conductivity of silicon.
(2) The dependence $\sigma(P_x)$ agrees qualitatively with the dependence of [22]. In both cases the silicon conductivity rises monotonically with increasing elastic stress.
(3) The general trend of the conductivity versus the stress in dynamic measurements is in remarkable agreement with the static measurements by Bundy and Kasper [16] (the monotonic rise with increasing stress, the break at 12–13 GPa).
(4) The conductivities of metallic silicon for dynamic and static compressions differ considerably. For $P_x \approx 15$ GPa the static compression conductivity is five times higher than the shock compression conductivity.

3.2. Behaviour on release

Investigation of silicon during release provides important information on the nature of the high pressure phase. The conductivity can be found for the temporal range up to the arrival of non-axial waves. A detailed comparison between the dependences of the conductivity and the stress on time allows one to find the stress dependence of the conductivity during release. The release dependences $\sigma(P_x)$ obtained for a number of experiments are shown in figures 3 and 4 by the chain curves.

On releasing from the metallic state, the conductivity of silicon decreases. As can be seen from figure 4 the conductivity during release proves to be very close to the conductivity under shock compression. This attests to the reversibility of the physical state of silicon up to the break point $P_x \approx 12$ GPa. Unloading to the lower stresses is accompanied with conservation or only slight change of the conductivity. The conductivity deviation between shock compression and release goes up to several orders of magnitude. Thus, the electrical conductivity shows a large hysteresis. The conductivity hysteresis was noticed in static compression [16] (see figure 3). Thus the behaviours of silicon under shock and static compression are qualitatively similar, though there are obvious quantitative distinctions.

Experiments with a metallic impacter allow one to consider with more certainty the silicon state at complete release. Figure 2(c) gives a record of a similar experiment. As seen from the figure, in the stress release there is conservation of the metallic phase of silicon at that time. This conclusion is also confirmed by additional experiments (not included in table 1) on thin impacters. When employing an impacter 0.8 mm thick, the duration of the stress pulse is so short (<100 ns) that it cannot be recorded with a manganin gauge. The moving impacter produces electromagnetic disturbance that prevents one from obtaining the specimen conductivity reliably. Moreover, the voltage record, which is very similar to figure 2(c), unambiguously demonstrates the onset of high conductance and its conservation on release for at least several microseconds. The mechanical fracture of the measuring cell prevents further observation of the specimen state.

Experiment No 590 (shock stress $P_x \approx 10.5$ GPa) shows temporal conservation of the high conductivity (figure 4). In contrast, experiments Nos 544, 620 corresponding to the lower shock stress (7.5 GPa) provide a qualitatively different dependence. The corresponding release

curves in figure 3 practically merge with the dependence $\sigma(P_x)$ for compression. The same behaviour is inherent in unloading states with lower shock stress. The qualitative difference in behaviour on releasing from the stresses 7.5 GPa and 10–10.5 GPa indicates different contents of the metallic phase at these shock stresses.

So, the array of experimental data is indicative of the metastability of the high stress phase. The lifetime of the metallic phase exceeds the characteristic time of the shock wave experiment anyway (several microseconds).

4. Discussion

4.1. Threshold stress of the metallic transition

As seen from figure 4, there is appreciable conductivity at a shock stress of about 10 GPa. The $\sigma(P_x)$ dependence can be seen as evidence of a percolation phenomenon in the two-component medium consisting of semiconductor and metallic phases. The effective conductivity of the medium depends on its composition and the topology of the metallic nuclei [47]. If the form of the nucleus is unknown *a priori*, at present the amount of metallic phase is difficult to judge. Shock compression of silicon at $P_x \approx 10$–10.5 GPa provides a noticeable concentration of the metallic phase anyway. Therefore it may be concluded that a stress of about 10 GPa is the threshold stress of the metallization. Above the stress 12 GPa the conductivity of silicon changes rather slightly. This indicates metallization of most of the specimen.

Let us compare the threshold stress of the metallization with known data on the phase transition in silicon. The value found is less than the transition stresses 13.3 GPa [21] and 13.4 GPa [24] but close to the stresses 11.2 GPa [19] and 10 GPa [20]. On the basis of a summary of the experimental data [24] one can deduce that the specific volume change $(V_0 - V_T)/V_T$ is about 8.2% at the shock stress of 10 GPa (V_0 is the initial specific volume, V_T is the specific volume corresponding to the onset of the phase transformation). This value agrees closely with that obtained by the x-ray diffraction method under static compression [1, 5, 6]. The detection of orthorhombic [10] and simple hexagonal [4–6, 10] phases of silicon allows one to fit the known shock data. Now it seems most plausible that the break of the wave profiles registered at $P_x \approx 10$–11 GPa [19, 20] was caused by a transition to the metallic β-tin phase and the break at $P_x \approx 13$–14 GPa [20, 21, 24] was due to the onset of the orthorhombic phase. The complexity of detecting the shock wave profiles in silicon is caused by the proximity of the shock stresses and the small volume changes corresponding to the transformations from β-tin to orthorhombic phase and thereafter to simple hexagonal phases [10]. Note that only direct measurements of the conductivity allow one to clarify the situation and to find the metallic transition stress. At stress higher than 11–12 GPa the phases are metallic; therefore the following transitions are not accompanied by a substantial change of the conductivity and are undetected by our technique.

It should be mentioned that some ambiguity of this treatment is concerned with the conductivity hysteresis. As the conductivity obtained in the first compression of silicon is conserved at release, determination of the threshold stress according to figure 4 may be rather debatable. Stresses for the first shock wave in silicon P_x^1 are shown in table 1. They were estimated from the stress in a dielectric P_x by the impedance matching method. For most of the experiments the stress P_x^1 exceeds the equilibrium stress in silicon P_x. With $P_x > 15$ GPa the deviation is moderately high. The stress P_x^1 should be considered as an upper estimate for the arising uncertainty. In any case, the hysteresis effect does not affect the conclusion about the proximity of the threshold stresses for dynamic and static compressions as well as the correspondence of the metallic transition to the lower shock stress.

4.2. The superdefect state of metallic silicon

The significant discrepancy between the metallic conductivities under dynamic and static compressions is unexpected and needs to be clearly explained. In any case, it is indicative of an essential distinction between the silicon states at different loading conditions. The distinction may be caused by shock heating or the generation of crystal structure defects.

Let us write the difference in resistivity in the form of two summands describing the effects of the shock heating and the shock generation of defects:

$$\rho_{\text{shock}} - \rho_{\text{static}} \approx \Delta\rho_T + \Delta\rho_{\text{def}}.$$

For $P_x \approx 15$ GPa the relative change of the resistivity is $(\rho_{\text{shock}} - \rho_{\text{static}})/\rho_{\text{static}} \approx 4$.

The effect of heating on the conductivity can be evaluated. The temperature of monocrystalline silicon under shock compression is calculated using the energy equation [48] and the Hugoniot adiabat [24]. The specific heat is taken from the Debye theory. The volume dependence of the Grüneisen factor γ is assumed to be of the form $\gamma V_0 = \gamma_0 V$, where γ_0 is the Grüneisen factor under standard conditions. The following values are used in the calculations: the initial temperature $T_0 = 293$ K; $\gamma_0 = 0.74$; the Debye temperature $\theta = 625$ K [49]. The shock heating turns out to be quite brief: $\Delta T \approx 75$ K for $P_x = 15$ GPa and $\Delta T \approx 105$ K for $P_x = 20$ GPa. This procedure ignores the hydrodynamic relaxation caused by shock reverberation in the cell. Accounting for reverberation produces $\Delta T \approx 121$ K for the stress $P_x = 20$ GPa. For the purposes of the present research this deviation can be neglected.

Using the temperature and the thermal resistance factor $\alpha \approx 5 \times 10^{-3}$ C^{-1} [15, 16, 50] obtained for metallic silicon, one can conclude that the relative change of the resistivity caused by the shock heating is $\Delta\rho_T/\rho_{\text{static}} \approx 0.4$ under a stress of 15 GPa. Thus the relative change of the resistivity caused by the defects is $\Delta\rho_{\text{def}}/\rho_{\text{static}} \approx 3.6$. Consequently, the heating effect is quite slight; the main contribution to the resistivity deviation is caused by the generation of crystal structure defects.

Let us compare the isothermal resistivity change $\Delta\rho_{\text{def}}/\rho_{\text{static}}$ with those for metals shocked in the same stress range: 0.12 (copper), 0.16 (iron) [36], 0.1–0.2 (silver) [51]. The isothermal resistivity change of metallic silicon proves to be more than 20 times larger than those for the typical metals. This means that the crystal structure arising during the phase transition under shock loading has a higher degree of disorder.

At present, increase of the metal resistivity under plastic deformation is recognized to be mandatory for generation of point defects [52]. As a matter of fact, for most metals the vacancies have the least energy and represent the most economical way of producing crystal defects. On the basis of this, let us suppose that the defects of metallic silicon are caused mainly by vacancies. The vacancy concentration can be estimated using the formula $n_{\text{v}} \approx \Delta\rho_{\text{def}}/\rho_{\text{v}}$ where ρ_{v} is the metal resistivity caused by a defect concentration of 1%. The vacancy resistivity ρ_{v} is unachievable for metallic silicon; therefore for the estimation we use the value ρ_{v} under standard conditions for tin: 3.3×10^{-6} Ω cm/at.% [53]. White tin has a tetragonal crystal structure similar to that of the metallic phase Si II. Note that the vacancy resistivity of aluminium (the element next to silicon in the periodic table) has the close value $\rho_{\text{v}} \approx 3.4 \times 10^{-6}$ Ω cm/at.% [53]. The silicon resistivity under static pressure of 15 GPa is 6×10^{-6} Ω cm [16]; the isothermal resistivity under shock loading derived from our experiments is 2.2×10^{-5} Ω cm. Thus, the vacancy concentration in metallic silicon is found to be $n_{\text{v}} \approx 0.05$. This value exceeds by more than one order of magnitude the vacancy concentration in shocked silver: $n_{\text{v}} \sim 10^{-3}$ [51]. Also, it exceeds by more than three orders of magnitude the vacancy concentration in metals undergoing low velocity deformation ($n_{\text{v}} \approx 10^{-5}$ at the deformation $\varepsilon = 0.1$) [52]. The equilibrium concentration of crystal defects is estimated as $n_{\text{v}}^{\text{e}} \sim \exp(-EkT)$ where E is the energy of the defect, k is the

Boltzmann factor [52]. For values $E \approx 1$ eV, $T = 349$ K (the shock temperature at the stress $P_x = 15$ GPa) the estimation gives $n_v^e \sim 10^{-7}$. The defect concentration in the shock obtained by this means exceeds the equilibrium one by more than five orders of magnitude. These estimations provide evidence that the state of shocked metallic silicon is highly defective and far from equilibrium. It can be characterized as a superdefect state as compared with the state for classic metals.

5. Conclusions

The present experiments represent the first successful attempt to study the shock metallization of silicon by directly measuring the electrical conductivity. The technique presented allowed us to solve the problem of measuring the conductivity in the dielectric–metal transition in a shock wave, which was known of even in the early 1960s. The technique reduces the current relaxation time to its diffusion limit, which improves the temporal resolution and allows one to measure the conductivity corresponding to classic metals.

As the stress P_x rises, the silicon conductivity σ increases monotonically by over five orders of magnitude and reaches the value $\sigma \approx 4.5 \times 10^4\ \Omega^{-1}\ \mathrm{cm}^{-1}$ under the stress $P_x \approx 23$ GPa. The $\lg \sigma(P_x)$ dependence comprises two parts: a steep increase and a 'plateau'. A similar form of the dependence was observed early on under dynamic loading for sulfur [38] and hydrogen [40]. Obviously it may be considered as typical for the dielectric–metal transition.

The 'plateau' conductivity corresponds to the metallic state of silicon; it does not depend on the compression regime, the initial impurity or the conductivity type. The 'plateau' conductivity is close to those of such metals as lead, vanadium, strontium and caesium. The occurrence of the metallic phase arises at the shock stress $P_x \approx 10$ GPa; most of the specimen becomes metallic at $P_x \approx 12$ GPa. The threshold metallization stress for shock compression is close to that for static compression [3, 5, 6, 8, 10]. This is indicative of the quasihydrodynamic state of shocked metallic silicon. The threshold metallization stress corresponds to the break of the shock profile registered early on at $P_x = 10$–11 GPa [19, 20].

The general trend of the $\lg \sigma(P_x)$ dependence under dynamic conditions is in remarkable agreement with the static measurements by Bundy and Kasper [16] (the monotonic rise with increasing stress, the break position). However, the conductivity values for metallic silicon for shocked and static compressions differ greatly. The temperature effect proves to be small and the conductivity deviation is mainly caused by shock generation of crystal structure defects. In the limited time of the observation the defects have no time to diffuse to specimen surfaces and they remain 'frozen'. An estimation of the vacancy concentration provides a value of 0.05 per lattice atom. The value exceeds that for the classic metals by more than one order of magnitude; it also exceeds the equilibrium defect concentration by five orders of magnitude. The metallic state of silicon in a shock wave is highly defective and far from equilibrium.

The present data are the first ones giving the time-resolved defect content of brittle solids in a shock wave. The results obtained are indicative of essential distinctions between the deformation mechanisms of brittle solids and the classic metals under shock loading.

The release tests indicate a severe asymmetry of the forward and reverse transitions. The high stress phase proves to be metastable for characteristic times of the shock experiment. It is retained for some time on complete release of the specimen.

References

[1] Jamieson J 1963 *Science* **139** 762
[2] Wentorf R W and Kasper J S 1963 *Science* **139** 338
[3] Werner A, Sanjurjo J A and Cardona M 1982 *Solid State Commun.* **44** 155
[4] Olijnyk H, Sikka S K and Holzapfel W B 1983 *Phys. Lett.* A **103** 137

[5] Hu J Z and Spain I L 1984 *Solid State Commun.* **51** 263
[6] Hu J Z, Merkle L D, Menoni C S and Spain I L 1986 *Phys. Rev.* B **34** 4679
[7] Zhao Y X, Buehler F, Sites J R and Spain I L 1986 *Solid State Commun.* **59** 679
[8] Duclos S J, Vohra Y K and Ruoff A L 1987 *Phys. Rev. Lett.* **58** 775
[9] Duclos S J, Vohra Y K and Ruoff A L 1990 *Phys. Rev.* B **41** 12021
[10] McMahon M I, Nelmes R J, Wright N G and Allan D R 1994 *Phys. Rev.* B **50** 739
[11] Christensen N E, Novikov D L, Alonso R E and Rodriguez C O 1999 *Phys. Status Solidi* b **211** 5
[12] Chang K J and Cohen M L 1985 *Phys. Rev.* B **31** 7819
[13] Weinstein B A and Piermarini G J 1975 *Phys. Rev.* B **12** 1172
[14] Welber B, Kim C K, Cardona M and Rodriguez S 1975 *Solid State Commun.* **17** 1021
[15] Bundy F P 1964 *J. Chem. Phys.* **41** 3809
[16] Bundy F P and Kasper J S 1970 *High Temp.—High Pressures* **2** 429
[17] Drickamer H G 1970 *Rev. Sci. Instrum.* **41** 1667
[18] Erskine D, Yu P Y, Chang K J and Cohen M L 1986 *Phys. Rev. Lett.* **58** 775
[19] Pavlovskii M N 1968 *Sov. Phys.—Solid State* **9** 2514
[20] Gust W H and Royce E B 1971 *J. Appl. Phys.* **42** 1897
[21] Coleburn N L, Forbes J W and Jones H D 1972 *J. Appl. Phys.* **43** 5007
[22] Rosenberg G 1980 *J. Phys. Chem. Solids* **41** 561
[23] German V N and Poduretc A M 1981 *Fiz. Tverd. Tela* **23** 246
[24] Goto T, Sato T and Syono Y 1982 *Japan. J. Appl. Phys.* **21** L369
[25] Zaporozhetc Yu B, Mintsev V B and Fortov V E 1986 *Detonation and Shock Waves* (Chernogolovka: OIHF) p 82 (in Russian)
[26] Gilev S D and Trubachev AM 1982 *Sov. Tech. Phys. Lett.* **8** 396
[27] Bichenkov E I, Gilev S D, Ryabchun A M and Trubachev A M 1987 *Megagauss Technology and Pulse Power Application* ed C M Fowler, R S Caird and D J Erickson (New York: Plenum) p 89
[28] Nagayama K and Mashimo T 1987 *J. Appl. Phys.* **61** 4730
[29] Bichenkov E I, Gilev S D and Trubachev A M 1989 *J. Appl. Mech. Tech. Phys.* **30** 291
[30] Gilev S D 1997 *Tech. Phys.* **42** 107
[31] Barmin A A and Prishepenko A B 1994 *Megagauss Magnetic Field Generation and Pulsed Power Application* ed M Cowan and R B Spielman (New York: Nova Science) p 35
[32] Gilev S D and Trubachev A M 1998 *Shock Compression of Condensed Matter 1997* ed S C Schmidt, D P Dandekar and J W Forbes (New York: AIP) p 777
[33] Gilev S D and Trubachev A M 1999 *Phys. Status Solidi* b **211** 379
[34] Brish A A, Tarasov M S and Tsukerman V A 1960 *Sov. Phys.—JETP* **11** 15
[35] Styris D L and Duvall G E 1970 *High Temp.—High Pressures* **2** 477
[36] Keeler R N 1971 *Physics of High Energy Density* ed P Caldirola and H Knoepfel (New York: Academic) p 106
[37] Yakushev V V 1978 *Combust. Explos. Shock Waves* **14** 131–46
[38] Nabatov S S, Dremin A N, Postnov V I and Yakushev V V 1979 *JETP Lett.* **29** 370
[39] Nabatov S S, Dremin A N, Postnov V I and Yakushev V V 1979 *Pis. Zh. Tekh. Fiz.* **5** 143
[40] Nellis W J, Weir S T and Mitchell A C 1999 *Phys. Rev.* B **59** 3434
[41] Dremin A N and Kanel G I 1972 *Combust. Explos. Shock Waves* **8** 120
[42] Gilev S D 2001 *Combust. Explos. Shock Waves* **37** 230
[43] Al'tshuler L V, Bakanova A A, Dudoladov I P, Dynin E I, Trunin R F and Chekin B S 1981 *J. Appl. Mech. Tech. Phys.* **22** 145
[44] Bloomquist D D, Duvall G E and Dick J J 1979 *J. Appl. Phys.* **50** 4838
[45] McQueen R G, Marsh S P, Taylor J W, Fritz J N and Carter W J 1970 *High-Velocity Impact Phenomena* ed R Kinslow (New York: Academic) chapter 7 p 294
[46] Shehter B I and Shunko L A 1973 *Combust. Explos. Shock Waves* **9** 519
[47] Clerk J P, Giraud G, Laugier J M and Luck J M 1990 *Adv. Phys.* **39** 191
[48] Duvall G E 1973 *Dynamic Response of Materials to Intense Impulsive Loading* ed P C Chou and A K Hopkins (Ohio: Air Force Materials Laboratory) p 89
[49] Zharkov V N and Kalinin V A 1968 *The Equation of State of Solids under High Pressure and Temperature* (Moscow: Nauka) (in Russian)
[50] Dunn K J and Bundy F P 1980 *J. Appl. Phys.* **51** 3246
[51] Dick J J and Styris D L 1975 *J. Appl. Phys.* **46** 1602
[52] Cahn R W and Haasen P 1983 *Physical Metallurgy* (Amsterdam: North-Holland)
[53] Damask A C and Dienes G J 1963 *Point Defects in Metals* (New York: Gordon and Breach)